

A Model for Two-Channel Kondo Effect in CNT Quantum Dot

I. Kuzmenko, T. Kuzmenko and Y. Avishai

Department of Physics, Ben-Gurion University of the Negev, Beer-Sheva, Israel

(Dated: February 29, 2024)

Over-screened Kondo effect is feasible in carbon nanotube quantum dot junction hosting a spin $\frac{1}{2}$ atom with single s -wave valence electron (e.g Au). The idea is to use the two valleys as two symmetry protected flavor quantum numbers $\xi = \mathbf{K}, \mathbf{K}'$. Perturbative RG analysis exposes the finite weak-coupling two-channel fixed point, where the Kondo temperature is estimated to be around $0.5 \div 5$ K. Remarkably, occurrence of two different scaling regimes implies a non-monotonic dependence of the conductance as function of temperature.

Introduction About three and a half decades ago, it was noticed [1] that when a magnetic impurity of spin $1/2$ is over-screened by two identical conducting electron channels, the many-body physics is characterized by a non-Fermi-liquid fixed point at temperature T smaller than the Kondo temperature T_K . Experimentally, this phenomenon, referred to as two-channel Kondo effect (2CKE), is characterized by unusual physics as $T \rightarrow 0$, such as non-zero entropy, divergence of susceptibility and others [2–6]. Realizing 2CKE in quantum dot with odd electron occupation is remarkably elusive due to channel anisotropy emerging from inter-channel co-tunneling processes. To remedy this instability, a suppression of inter-channel co-tunneling is attempted [7] where the interference is suppressed by Coulomb blockade.

In this work we use a novel approach to avoid channel mixing using a CNTL-CNTQDA-CNTR junction as shown in Fig. 1(a). Here CNTL, CNTR are semi infinite carbon nano tube (CNT) left and right leads and CNTQDA is a short CNT quantum dot with an atom A with s -wave valence electron of spin $S_A = \frac{1}{2}$ implanted on its axis. The two valleys \mathbf{K} and \mathbf{K}' serve as two symmetry protected flavor quantum numbers $\xi = \mathbf{K}, \mathbf{K}'$. The

CNTQDA is gated such that its (neutral) ground state consists of the caged atom ket $|M_A = \pm \frac{1}{2}\rangle$ and its lowest excited (charged) states are singlet and triplet (defined explicitly below), formed as proper combinations of basic states $|M_A\rangle \otimes |\xi\sigma\rangle$, where $|\xi\sigma\rangle$ is a CNTQD electron of flavor ξ and spin projection $\sigma = \pm \frac{1}{2}$. The Anderson model hybridizes lead and dot electrons with the same flavor and spin projection, and the Schrieffer-Wolf transformation, while mixing spin projections does not mix flavors, thereby realizing a two-channel Kondo physics. Perturbative RG analysis exposes the finite weak-coupling two-channel fixed point, where the Kondo temperature is estimated to be around $0.5 \div 5$ K.

It should be stressed that a junction with CNTQD containing odd number of electrons in the ground state albeit *without a caged atom*, will *not* display the 2CKE, because an electron with flavor quantum number ξ can tunnel from the dot to the lead, and be replaced by another electron with flavor quantum number ξ' . As a result, flavor is not a good quantum number and flavor (channel) mixing results in crossover to the ordinary (single-channel) Kondo effect [8, 9].

Implanting Gold Atom on the CNT axis

A crucial ingredient in the present analysis is the feasibility of caging an atom such as Au (for example) on the CNT axis x as in Fig. 1a. Here we briefly describe the underlying construction. Technical aspects of atomic physics are detailed in the Supplemental Material (SM). Consider first an infinitely long CNT (along the x axis) and let $\mathbf{q} = \mathbf{k} - \mathbf{K}$ or $\mathbf{q} = \mathbf{k} - \mathbf{K}'$. For an electron at small $|\mathbf{q}|$, the energy dispersion is [10, 11], $\epsilon_{qm} = \sqrt{(\hbar v q)^2 + (m + \nu)^2 \Delta_0^2}$, where $\mathbf{q} = (q, \frac{m + \nu}{r_0})$, q is the wave number in the CNT direction and m is the orbital quantum number ($m = 0, \pm 1, \pm 2, \dots$), $\Delta_0 = \frac{\hbar v}{r_0}$, $v \sim 10^8$ cm/sec is the group velocity of electrons in a metallic CNT [10, 11] and r_0 is the CNT radius. The quantum number ν is 0 for metallic CNT or $\pm \frac{1}{3}$ for semiconductor CNT [10, 11]. In what following, ν will be tuned to be non-zero, implying a semiconductor CNT.

Now let us check under what conditions it is possible to implant and stabilize a gold atom on the CNT axis. Denoting the van der Waals interaction between the Au and C atoms a distance Y apart by $V_w(Y)$, the van der Waals

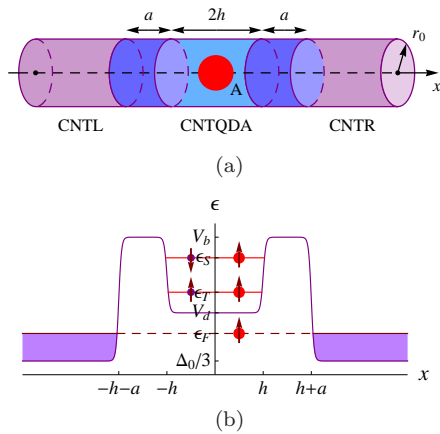


FIG. 1: CNTL-CNTQDA-CNTR junction. (a) Schematic geometry of the junction including semi-infinite left and right leads, separated from a quantum dot of length $2h$ (that hosts a spin $1/2$ atom A) by two barriers of width a . (b) Low energy levels of the quantum dot with (from below) the caged atom, followed by triplet and singlet atom-electron states.

interaction of the Au atom with the *entire* CNT is then,

$$V(\mathbf{R}) = \sum_{\alpha=A,B} \sum_{\mathbf{R}_\alpha} V_w(|\mathbf{R} - \mathbf{R}_\alpha|), \quad (1)$$

where \mathbf{R} is the position of the Au atom, $\mathbf{R}_{A,B}$ are the positions of atoms C on sub-lattices A, B . Due to cylindrical symmetry, $V(\mathbf{R}) = V(R, X)$ depends on X (along which it is periodic) and R (radial variable). Plots of

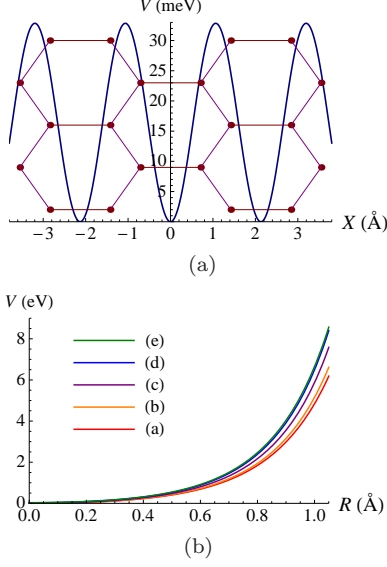


FIG. 2: (Color online) (a) Van der Waals potential $V(0, X)$, Eq. (16). The purple dots and lined denote the lattice of the CNT. (b) Van der Waals potential $V(R, X)$ as a function of R for different values of X : Curves a,b,c,d,e correspond to $X = 0.25(m-1)X_1$, $m = 1, 2, 3, 4, 5$.

$V(0, X)$ and $V(R; X)$ [as calculated in the SM based on realistic parametrization of $V_w(Y)$], are displayed in Fig. 2a, b for a zigzag CNT with radius $r_0 = 3.13$ Å. $V(R, X)$ has minima and saddle points at $(0, X_n^{\min}), (0, X_n^{\text{sad}})$, ($n = 0, \pm 1, \pm 2, \dots$)

$$X_n^{\min} = 2nX_1, \quad X_n^{\text{sad}} = (2n+1)X_1, \quad X_1 = \frac{3a_0}{4\sqrt{3}}. \quad (2)$$

The height of the tunnel barriers between two minima is

$$W_b = V(0, X_n^{\text{sad}}) = 32.8 \text{ meV}. \quad (3)$$

Expansion of $V(R, X)$ around the minima $(0, X_n^{\min})$ shows that, to second order, the Au atom moves in an anisotropic harmonic oscillator potential with spring constants $K_x = 0.072 \text{ eV/Å}^2$, $K_r = 1.117 \text{ eV/Å}^2$. The energy of the ground state in this harmonic potential is about 5.5 meV, much smaller than the barrier height W_b . Moreover, the harmonic radius $a_x \approx 0.11$ Å, is much smaller than $X_1 = 1.07$ Å, so that the harmonic approximation is self-consistent and the picture of well localized Au atom on the CNT axis makes sense.

Gating a Quantum Dot with implanted Magnetic Atom: To get a CNTL-CNTQDA-CNTR junction as in Fig. 1(a)

the infinite CNT is now gated by the potential:

$$V_g(x) = -\frac{\Delta_0}{3} - V_0 \vartheta(|x| - h - a) + V_d \vartheta(h - |x|) + V_b \vartheta(|x| - h) \vartheta(h + a - |x|), \quad (4)$$

where $V_b > V_d > 0$ and $V_0 > 0$. This gate divides the CNT into 5 intervals whose geometry and energy levels are displayed in Figs 1(a) and 1(b):

- 1) $|x| > h + a$, (left and right leads): Here the Fermi energy ϵ_F is over the bottom of the conduction band.
- 2) $h + a > |x| > h$, the left and right barriers.
- 3) $|x| < h$, (the QD): Here the Fermi energy is below the single-electron level, so that the ground state of the QD hosts solely the spin 1/2 caged atom while its excited states contain one electron and the caged atom. Together, they form singlet (S) and triplet (T) states. The exchange interaction between the atom and the electron is considered in the SM (based on Hund rules, as it is quite a standard aspect of atomic physics). It is shown that the singlet-triplet splitting $V_{\text{exch}} = \epsilon_T - \epsilon_S$ due to the direct exchange term is $V_{\text{exch}} = -43.3 \text{ meV}$, while the indirect exchange term is absent. Since $V_{\text{exch}} < 0$ the exchange interaction is *ferromagnetic* and the corresponding energies satisfy $\epsilon_S > \epsilon_T$, see Fig. 1(b).

Notations for Anderson model: 1) $c_{\alpha q \xi \sigma}$ are electron annihilation operators in the leads $\alpha = L, R$, with momentum q , energy $\epsilon_q = \sqrt{(\hbar v q)^2 + \frac{1}{9} \Delta_0^2}$, flavour $\xi = \mathbf{K}, \mathbf{K}'$ and spin projection $\sigma = \pm \frac{1}{2}$. 2) For a lead of length L the electron DOS is $\rho(\epsilon) = \frac{1}{L} \sum_k \delta(\epsilon - \epsilon_k) = \frac{\vartheta(\epsilon - \frac{1}{3} \Delta_0)}{\pi \hbar v_\epsilon}$ where $v_\epsilon = \frac{v}{\epsilon} \sqrt{\epsilon^2 - \frac{1}{9} \Delta_0^2}$ is the group velocity. 3) $d_{\xi \sigma}$ is the annihilation operator for dot electron of flavour ξ and spin projection σ . 4) $|M_A\rangle$ is a dot atom state with spin projection $M_A = \uparrow, \downarrow$ and energy $\epsilon_{M_A} = 0$. 5) The atom (doublet) and atom-electron singlet and three triplet states of the dot are collectively denoted as $|\Lambda\rangle = |M_A\rangle, |S\xi\rangle, |\uparrow\xi\rangle, |0\xi\rangle, |\bar{1}\xi\rangle$. The triplet states are, $|\uparrow\xi\rangle = d_{\xi\uparrow}^\dagger |\uparrow\rangle$, $|0\xi\rangle = \frac{1}{\sqrt{2}} \{d_{\xi\uparrow}^\dagger |\downarrow\rangle + d_{\xi\downarrow}^\dagger |\uparrow\rangle\}$, $|\bar{1}\xi\rangle = d_{\xi\downarrow}^\dagger |\downarrow\rangle$, and the singlet state is $|S\xi\rangle = \frac{1}{\sqrt{2}} \{d_{\xi\uparrow}^\dagger |\downarrow\rangle - d_{\xi\downarrow}^\dagger |\uparrow\rangle\}$.

6) The dot Hubbard operators are $X^{\Lambda, \Lambda'} \equiv |\Lambda\rangle\langle\Lambda'|$. The dot electron operators $d_{\xi \sigma}$ defined in 3) are expressible in terms of $X^{M_A, S\xi}, X^{M_A, \uparrow\xi}, X^{M_A, 0\xi}, X^{M_A, \bar{1}\xi}$ as, $d_{\xi \sigma} = X^{\sigma, 1\xi} + \frac{1}{\sqrt{2}} \{X^{\bar{\sigma}, 0\xi} + 2\sigma X^{\bar{\sigma}, S\xi}\}$, ($\bar{\sigma} \equiv -\sigma$).

Anderson and Kondo Hamiltonians The Anderson Hamiltonian of the CNTL-CNTQDA-CNTR junction is:

$$H = H_L + H_R + H_D + H_T, \quad (5a)$$

$$H_\alpha = \sum_{q\xi\sigma} \epsilon_q c_{\alpha q \xi \sigma}^\dagger c_{\alpha q \xi \sigma}, \quad (5b)$$

$$H_D = \sum_{\xi} \left\{ \epsilon_T \sum_m X^{m\xi, m\xi} + \epsilon_S X^{S\xi, S\xi} \right\}, \quad (5c)$$

$$H_T = \sum_{\alpha q \xi \sigma} t_{\epsilon_q} \left\{ c_{\alpha q \xi \sigma}^\dagger d_{\xi \sigma} + d_{\xi \sigma}^\dagger c_{\alpha q \xi \sigma} \right\}, \quad (5d)$$

Here $t_\epsilon = t_F \sqrt{\frac{v_\epsilon}{v_F}}$, $v_F = v_{\epsilon_F}$, and t_F is the tunneling rate for electrons at the Fermi level. The energies of the triplet and singlet states, ϵ_T and ϵ_S , satisfy the properties, $\epsilon_S > \epsilon_T > \epsilon_F$, (see Fig. 1(b)). Applying the Schrieffer-Wolf transformation leads to the Kondo Hamiltonian

$$H_K = \sum_{\xi qq'} \left\{ K_{\epsilon_q \epsilon_{q'}} n_{\xi, qq'} + J_{\epsilon_q \epsilon_{q'}} (\mathbf{S} \cdot \mathbf{s}_{\xi, qq'}) \right\}, \quad (6)$$

$$n_{\xi, qq'} = \sum_{\alpha \alpha' \sigma} c_{\alpha q \xi \sigma}^\dagger c_{\alpha' q' \xi \sigma},$$

$$\mathbf{s}_{\xi, qq'} = \frac{1}{2} \sum_{\alpha \alpha' \sigma \sigma'} c_{\alpha q \xi \sigma}^\dagger \boldsymbol{\tau}_{\sigma \sigma'} c_{\alpha' q' \xi \sigma'},$$

$$\mathbf{S} = \frac{1}{2} \sum_{\sigma \sigma'} \boldsymbol{\tau}_{\sigma \sigma'} X^{\sigma \sigma'}.$$

The couplings $K_{\epsilon \epsilon'}$ and $J_{\epsilon \epsilon'}$ are

$$K_{\epsilon \epsilon'} = \frac{3t_\epsilon t_{\epsilon'}}{4(\epsilon_T - \epsilon_F)} + \frac{t_\epsilon t_{\epsilon'}}{4(\epsilon_S - \epsilon_F)},$$

$$J_{\epsilon \epsilon'} = \frac{t_\epsilon t_{\epsilon'}}{\epsilon_T - \epsilon_F} - \frac{t_\epsilon t_{\epsilon'}}{\epsilon_S - \epsilon_F}. \quad (7)$$

In the special case $\epsilon_S = \epsilon_T$, H_K contains just a potential scattering which does not include spin-flipping. Since $\epsilon_T < \epsilon_S$, an anti-ferromagnetic spin-spin exchange interaction appears ($J > 0$). Eq. (6) describes two-channel Kondo scattering with dot spin $S = \frac{1}{2}$, so that it results in over-screening of the impurity spin.

Scaling equation and Kondo temperature: Employing the poor man's scaling technique to the Kondo Hamiltonian (6), one can see that only the dimensionless coupling $j_{\epsilon \epsilon'} = J_{\epsilon \epsilon'} \sqrt{\rho(\epsilon) \rho(\epsilon')} = \frac{t_\epsilon^2 (\epsilon_S - \epsilon_T) \vartheta(\epsilon - \frac{\Delta_0}{3}) \vartheta(\epsilon' - \frac{\Delta_0}{3})}{\pi \hbar v_F (\epsilon_S - \epsilon_F) (\epsilon_T - \epsilon_F)}$ renormalizes. Note that for $\epsilon, \epsilon' > \frac{1}{3} \Delta_0$, $j \equiv j_{\epsilon \epsilon'}$ does not depend on ϵ and ϵ' .

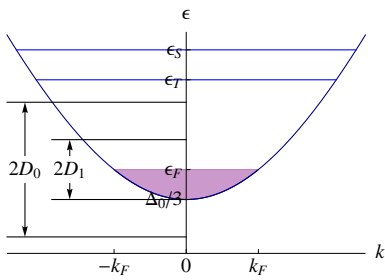


FIG. 3: (Color online) Two different intervals of the effective bandwidth D , $D_0 < D < D_1$ and $D < D_1$, where different RG regimes are expected.

The RHS of the scaling equation (see below) consists of the following terms, $j_{\epsilon \epsilon + D} j_{\epsilon + D \epsilon'}$, and $j_{\epsilon \epsilon' - D} j_{\epsilon - D \epsilon'}$, where ϵ and ϵ' are close to ϵ_F . The first term does not depend on energies and equals to j^2 , whereas the second term depends on the sign of $\epsilon_F - D - \frac{1}{3} \Delta_0$. For $\epsilon_F - D > \frac{1}{3} \Delta_0$, $j_{\epsilon \epsilon - D} j_{\epsilon - D \epsilon'} = j^2$, otherwise $j_{\epsilon \epsilon - D} j_{\epsilon - D \epsilon'} = 0$. As a result, for $D_0 > \epsilon_F - \frac{1}{3} \Delta_0$, there are two different regimes of the poor man's scaling procedure: $D_0 < D < D_1 =$

$\epsilon_F - \frac{1}{3} \Delta_0$ and $D < D_1$, as shown in Fig. 3. Within the first of them, $D_0 < D < D_1$, the energy level $\epsilon_F + D$ lies within the conduction band, whereas the energy $\epsilon_F - D$ is below the bottom of the conduction band. Within the second interval, $D < D_1$, both the energy levels, $\epsilon_F \pm D$, lie within the conduction band. This property effects on the RG procedure. We will consider the RG procedure within both of the intervals in turn.

First interval, $D_0 < D < D_1$: The second and third order diagrams containing hole lines (i.e., lines describing virtual electrons with energy $\epsilon - D$) vanish. Then scaling equations for k and j are,

$$\frac{\partial k}{\partial \ln D} = -k^2 - \frac{3j^2}{16}, \quad (8a)$$

$$\frac{\partial j}{\partial \ln D} = -2kj - \frac{j^2}{2}, \quad (8b)$$

where $D < D_0$ and the initial conditions are $k(D_0) = k_0$ and $j(D_0) = j_0$.

The solution of the set of equations (8) is,

$$k(D) = \frac{1}{4 \ln \left(\frac{D}{T_g} \right)} + \frac{3}{4 \ln \left(\frac{D}{T_f} \right)}, \quad (9a)$$

$$j(D) = \frac{1}{\ln \left(\frac{D}{T_g} \right)} - \frac{1}{\ln \left(\frac{D}{T_f} \right)}, \quad (9b)$$

where

$$T_g = D_0 \exp \left(-\frac{1}{g_0} \right), \quad T_f = D_0 \exp \left(-\frac{1}{f_0} \right),$$

$g_0 = k_0 + \frac{3}{4} j_0$ and $f_0 = k_0 - \frac{1}{4} j_0$. Since $g_0 > f_0$, $T_g > T_f$.

Provided that $D_1 > T_g$, the renormalization procedure (9) stops when D approaches D_1 and k and j approach $k_1 = k(D_1)$ and $j_1 = j(D_1)$. From this point, the second RG regime starts.

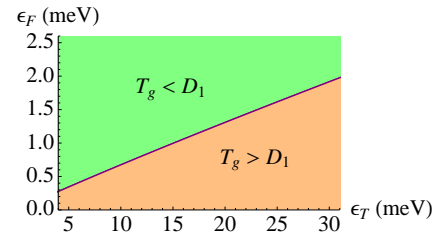


FIG. 4: (Color online) Intervals of ϵ_T and ϵ_F where $T_{K_1} < D_1$ (green area) or $T_{K_1} > D_1$ (orange area) separated by the purple curve where $T_{K_1} = D_1$. Here $\epsilon_S - \epsilon_T = 43.3$ meV.

Intervals of ϵ_F and ϵ_T where $T_g < D_1$ or $T_g > D_1$ are shown in Fig. 4. It is seen that there are some values $\epsilon_c(\epsilon_T)$ (purple curve) such that for $\epsilon_F > \epsilon_c(\epsilon_T)$, $T_g < D_1$ and the crossover from the single-channel to the two-channel Kondo regimes occurs in the weak coupling regime. When $\epsilon_F < \epsilon_c(\epsilon_T)$, $T_g > D_1$ and

the crossover from the single-channel to the two-channel Kondo regimes occurs in the strong coupling regime.

Second interval, $D < D_1$: The third order scaling equation for j is,

$$\frac{\partial j(D)}{\partial \ln D} = -j^2(D) + 2j^3(D), \quad (10)$$

and the initial condition is $j(D_1) = j_1$. Within this interval, the coupling k does not renormalizes. The solution of the scaling equation (10) is,

$$\frac{1}{j_1} - \frac{1}{j} + 2 \ln \left[\frac{j(1-2j_1)}{j_1(1-2j)} \right] = \ln \frac{D_1}{D}. \quad (11)$$

When D decreases, $j(D)$ renormalizes towards $j^* = \frac{1}{2}$, the fixed point value of j , and when D goes to 0, $j(D)$ goes to j^* . When $|j-j^*| \ll j^*$, the asymptotic expression for j is,

$$\frac{j-j^*}{j^*} = \frac{j^*-j_1}{j_1} \left(\frac{DT^*}{D_1 T_K} \right)^{j^*},$$

where the scaling invariants T_K and T^* are

$$T_K = D_1 \exp \left(-\frac{1}{j_1} \right), \quad T^* = D_1 \exp \left(-\frac{1}{j^*} \right). \quad (12)$$

Estimate of the couplings and Kondo temperature T_K :

The dimensionless couplings are,

$$j_0 = \frac{t_F^2(\epsilon_S - \epsilon_T)}{\pi \hbar v_F(\epsilon_S - \epsilon_F)(\epsilon_T - \epsilon_F)},$$

$$k_0 = \frac{t_F^2(3\epsilon_S + \epsilon_T - 4\epsilon_F)}{4\pi \hbar v_F(\epsilon_S - \epsilon_F)(\epsilon_T - \epsilon_F)}.$$

Here $\epsilon_S - \epsilon_T = 43.3$ meV (see the SM). The tunneling rate can be tuned by fitting the tunnel barrier height and width.

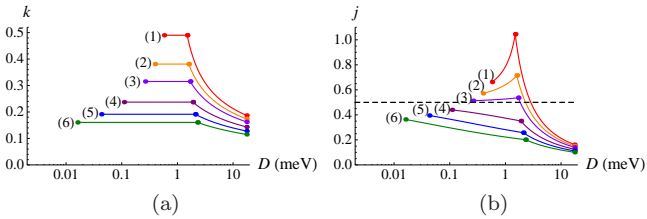


FIG. 5: (Color online) (a) k and (b) j as functions of D for $\epsilon_T = 19$ meV and different values of ϵ_F . Here $\epsilon_S - \epsilon_T = 43.3$ meV, $t_F \sqrt{k_F} = 0.35(\epsilon_T - \epsilon_F)$ and curves (1) – (6) correspond to $\epsilon_F = 1.5, 1.6, 1.7, 1.9, 2.1$ and 2.3 meV, respectively.

The dependence of the effective couplings k and j on the effective bandwidth D and the Fermi energy ϵ_F is shown in Fig.5 for the energy of the triplet state $\epsilon_T = 19$ meV. $k(D)$ as a function of D is shown in Fig.5(a) and renormalization of $j(D)$ is shown in Fig.5(b)

for different values of ϵ_F . It should be noted the behavior of the curves (1), (2) and (3) [$\epsilon_F \leq 1.7$ meV]: Within the interval $D_0 > D > D_1$, the effective coupling $j(D)$ increases to the value over j^* , and then within the interval $D < D_1$, $j(D)$ decreases approaching j^* . This behavior is unexpected, since in the standard two-channel Kondo model, the exchange coupling changes monotonically with D approaching j^* for $D \rightarrow 0$. The nonmonotonic behavior is caused by the crossover from the single-channel GR regime for $D > D_1$ to the two-channel RG regime for $D < D_1$.

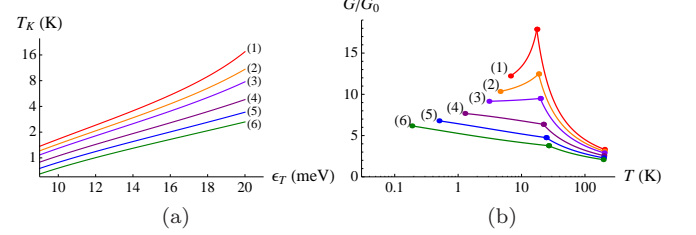


FIG. 6: (Color online) (a) T_K , Eq. (12), as a function of ϵ_T and different values of ϵ_F . (b) The conductance $G(T)$, Eq. (14) as function of T for $\epsilon_T = 19$ meV and different values of ϵ_F . For both panels, $t_F \sqrt{k_F} = 0.35(\epsilon_T - \epsilon_F)$, and curves (1) – (6) correspond to $\epsilon_F = 1.5, 1.6, 1.7, 1.9, 2.1$ and 2.3 meV, respectively. In panel (b), the dots from right to left correspond to D_0, D_1 and T_K , separating the RG regimes from one another.

The Kondo temperature T_K (12) is shown in Fig. 6a as a function of ϵ_T for $t_F \sqrt{k_F} = 0.35(\epsilon_T - \epsilon_F)$ and different values of ϵ_F . It is seen that T_K changes in between 0.5 K and 5 K for reasonable parameter values.

Conductance The non-linear tunneling conductance $G(T)$ of the CNTL-CNTQDA-CNTR junction in the weak coupling Kondo regime will now be calculated, employing perturbation RG formalism within the Keldysh non-equilibrium Green's function approach. The tunneling current from the left to the right lead is

$$I = \frac{ie}{\hbar} \sum_{\xi k k' \sigma \sigma'} \left\{ K_{\epsilon_k \epsilon_{k'}} \delta_{\sigma \sigma'} + \frac{J_{\epsilon_k \epsilon_{k'}}}{2} (\tau_{\sigma \sigma'} \cdot \mathbf{S}) \right\} \times \left(c_{Lk\xi\sigma}^\dagger c_{Rk'\xi\sigma'} - c_{Rk\xi\sigma}^\dagger c_{Lk'\xi\sigma'} \right). \quad (13)$$

Applying perturbation theory and the condition of invariance of the conductance with respect to the “rescaling” transformations, we get the following expression for the conductance,

$$G = \frac{\pi^2 G_0}{2} \left\{ k^2(T) + 3j^2(T) \right\}, \quad G_0 = \frac{e^2}{\pi \hbar}, \quad (14)$$

where $j(T)$ is given by Eqs. (9b) and (11) for $T > D_1$ and $T < D_1$, respectively; $k(T)$ is given by Eq. (9a) for $T > D_1$ and $k(T) = k(D_1)$ for $T < D_1$ [see also Fig. 5].

The conductance (14) as function of T is shown in Fig. 6b for $t_F \sqrt{k_F} = 0.35(\epsilon_T - \epsilon_F)$, $\epsilon_T = 19$ meV and different values of ϵ_F . Note the non-monotonic behavior of the

conductance for $\epsilon_F \leq 1.7$ meV [curves (1) – (3)]. This exotic behavior is caused by the non-monotonicity of $j(T)$ [see Fig. 5(b)]. In the standard 2CKE, $G(T)$ is monotonic, depending on the bare value j_0 of j . If $j_0 < j^* = \frac{1}{2}$, ($j_0 > j^*$), the conductance increases (decreases) monotonically with reducing T . Non-monotonicity of $G(T)$ exposed here is the result of the crossover between different RG scaling regimes.

Summary: In addition to suggesting a scheme for exposing 2CKE in an electronic transport system, the present scheme reveals a novel facet of the RG scaling framework, namely, the existence of two scaling regimes in which the running coupling constant behaves differently. This enables the physics of the 2CKE to be visible also in the weak coupling regime due to the non-monotonic behaviour of the conductance as function of temperature. Our analysis requires a versatile use of several physical disciplines. The properties of CNT are employed for the generation of decoupled electron channels, while the need to implant an atom on the axis of the CNT requires mastering of material science techniques. The elucidation of the van der Waals potential and the CNT and the calculation of the exchange constants are based on fundamental aspects of atomic physics, and the derivation of the Anderson and Kondo Hamiltonians touch upon the corner

sotnes of strongly correlated electrons.

Acknowledgement: The research of Y.A is partially supported by grant 400/12 of the Israel Science Foundation (ISF).

-
- [1] P. Nozières and A. Blandin, J. Physique **41**, 193 (1980).
 - [2] A.K. Mitchell, M. Becker, R. Bulla, Phys. Rev. B **84**, 115120 (2011).
 - [3] A.K. Mitchell, D.E. Logan, H.R. Krishnamurthy, Phys. Rev. B **84**, 035119 (2011).
 - [4] A.K. Mitchell, D.E. Logan, Phys. Rev. B **81**, 075126 (2010).
 - [5] D. Giuliano, A. Naddeo, A. Tagliacozzo, J. Phys. Cond. Mat. **16**, S1453 (2004).
 - [6] E. Lebanon, A. Schiller, F.B. Anders, Phys. Rev. B **68**, 155301 (2003).
 - [7] R.M. Potok, I.G. Rau, H. Shtrikman, Y. Oreg, and D. Goldhaber-Gordon, Nature **446**, 167 (2007).
 - [8] L.I. Glazman and M.E. Raikh, JETP Lett. **47**, 452 (1988).
 - [9] T. Kuzmenko, K. Kikoin, Y. Avishai, Europhys. Lett. **64**, 218 (2003).
 - [10] H. Ajiki and T. Ando, J. Phys. Soc. Jpn. **62**, 1255 (1993).
 - [11] H. Ajiki and T. Ando, J. Phys. Soc. Jpn. **65** 505 (1996).

SUPPLEMENTARY MATERIAL

In this Supplementary Material section we first expand upon the atomic-physics aspects of the CNTL-CNTQDA-CNTR junction and second, derive the scaling equations for the exchange coupling constants. In subsection I the van der Waals interaction between the gold atom and the CNT is derived based on the van der Waals interaction between the gold atom and a single carbon atom and on the geometry of the CNT. In subsection II the gold atom states in the CNT potential (derived in subsection I) are analyzed. Direct exchange interaction between the CNT itinerant electrons and the caged gold atom are discussed in subsection III providing us with the exchange constants that are required to arrive at the Kondo model of the main text. In subsection IV it is shown that the indirect exchange contribution is virtually negligible. Finally, in subsection V the scaling equations for the dimensionless couplings are derived. The reason for doing so is that these equations are not the standard ones encountered in the Kondo physics because, as indicated in the main text, there are two different scaling intervals, $D > D_1$ and $D < D_1$, corresponding to two different sets of scaling equations, and each regions requires a separate treatment.

I. Van der Waals Interaction between gold and carbon atoms forming CNT

When an atom of gold is implanted on the central axis of a CNT, there is van der Waals interaction between the gold and *all* the carbon atoms forming the CNT that need to be calculated. In order to calculate it we first write down the van der Waals interaction between the gold and a *single* carbon atom a distance Y apart, that reads,

$$V_w(y) = V_0 \left\{ \frac{1}{2} \frac{R_w^{12}}{Y^{12}} - \frac{R_w^6}{Y^6} \right\}, \quad (15)$$

where $R_w = 3.36$ Å is the equilibrium position and

$$V_0 = \frac{\epsilon_{Au}\epsilon_C}{\epsilon_{Au} + \epsilon_C} \frac{\alpha_{Au}\alpha_C}{r_w^6} = 32.6 \text{ meV},$$

where $\epsilon_{Au} = 9.2255$ eV or $\epsilon_C = 11.2603$ eV is the ionization energy for gold or carbon, $\alpha_{Au} = 36.1a_B^3 = 5.34$ Å³ or $\alpha_C = 11.7a_B^3 = 1.73$ Å³ is polarizability of the atom of gold or carbon ($a_B = 0.529$ Å is the Bohr radius). Then the

van der Waals interaction of the caged atom of gold with the CNT (see Fig. 7 for the geometry) is obtained just by summation,

$$V(\mathbf{R}) = \sum_{\mathbf{R}_A} V_w(|\mathbf{R} - \mathbf{R}_A|) + \sum_{\mathbf{R}_B} V_w(|\mathbf{R} - \mathbf{R}_B|), \quad (16)$$

where \mathbf{R}_A or \mathbf{R}_B are positions of atoms of sub-lattice A or B . Numerical calculations for $V(\mathbf{R})$ result its profile as displayed in Fig. 2 of the main text for a zigzag CNT with the chiral vector $\mathbf{c}_{8,0}$ and CNT radius $r_0 = 3.13 \text{ \AA}$. Essentially, the potential depends on two variables (cylindrical coordinates), X (along the CNT axis) and R (radial variable) and almost does not depend on the azimuthal angle ϕ . Hence we may write $V(\mathbf{R}) = V(R, X)$, which is, by construction, periodic in X . More concretely, for fixed X it increases quadratically with R , and for $R = 0$, $V(0, X)$ as a function of X has local minima X_n^{\min} and saddle points X_n^{sad} given by,

$$X_n^{\min} = 2nX_1, \quad X_n^{\text{sad}} = (2n+1)X_1, \quad X_1 = \frac{3a_0}{4\sqrt{3}} = 1.07 \text{ \AA}, \quad (17)$$

where n is integer. Numerical estimates show that neighboring minima are separated by tunnel barriers of height

$$W_b = V(0, X_n^{\text{sad}}) = 32.8 \text{ meV}. \quad (18)$$

Expansion of $V(R, X)$ around the minima $\mathbf{R}_n^{\min} = (X_n^{\min}, 0)$ up to quadratic powers yield,

$$V(R, X) \approx \frac{1}{2}K_x(X - X_n^{\min})^2 + \frac{1}{2}K_rR^2, \quad (19)$$

where $|X - X_n^{\min}| \ll X_1$ and $R \ll r_0$,

$$K_x = 0.072 \frac{\text{eV}}{\text{\AA}^2}, \quad K_r = 1.117 \frac{\text{eV}}{\text{\AA}^2}. \quad (20)$$

In what follows, we will assume that the gold atom performs small oscillations around the point $\mathbf{R} = (0, 0)$.

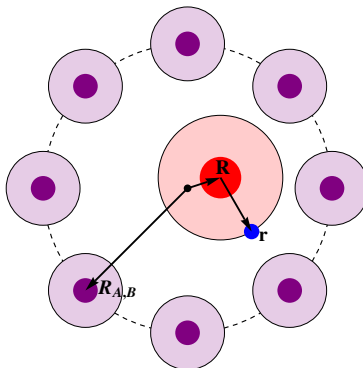


FIG. 7: (Color online) Atom of gold (red circle) and carbon atoms of the CNT (purple circles). Position of electron of the gold atom is \mathbf{r} , position of the gold nuclei is \mathbf{R} , positions of the carbon atoms are \mathbf{R}_A and \mathbf{R}_B .

II. Atomic Quantum States in the CNT Potential

Consider a neutral gold atom of mass M as a positively charged rigid ion (with filled shell) and one electron on the outer $6s$ orbital. The positions of the ion and the outer electron are respectively specified by vectors \mathbf{R} and \mathbf{r} [see Fig. 7]. In the adiabatic approximation (which is natural in atomic physics), the wave function of the atom is a product of the corresponding wave functions $\Psi^{\text{Au}}(\mathbf{R})$ and $\psi_6(\mathbf{r})$ describing the stationary states of the ion and the outer electron. In order to find the wave functions and energies of the gold atoms in the anisotropic potential well (19), we need to solve the following Schrödinger equation for $\Psi^{\text{Au}}(\mathbf{R})$,

$$-\frac{\hbar^2}{2M}\Delta\Psi^{\text{Au}}(\mathbf{R}) + V(\mathbf{R})\Psi^{\text{Au}}(\mathbf{R}) = \varepsilon\Psi^{\text{Au}}(\mathbf{R}). \quad (21)$$

Within the Harmonic approximation (19), the solutions of Eq. (21) are,

$$\Psi_{nm\ell}^{\text{Au}}(\mathbf{R}) = \Phi_{\nu m}(R) F_{\ell}(X) e^{im\phi}, \quad (22a)$$

where X , R and ϕ are cylindrical coordinates. Denoting $\rho \equiv R/a_r$, the radial wave function $\Phi_{nm}(R)$ is,

$$\Phi_{nm}(R) = \frac{1}{a_r \sqrt{\pi}} \sqrt{\frac{n!}{(n+|m|)!}} \rho^{|m|} L_{\nu}^{(|m|)}(\rho^2) e^{-\frac{\rho^2}{2}}, \quad (22b)$$

where $L_{\nu}^{(|m|)}$ is the generalized Laguerre polynomial, $n = 0, 1, 2, \dots$ and $m = 0, \pm 1, \pm 2, \dots$, and

$$a_r = \sqrt{\frac{\hbar\omega_r}{K_r}}, \quad \omega_r = \sqrt{\frac{K_r}{M_{\text{Au}}}}. \quad (22c)$$

Denoting $\zeta \equiv X/a_x$ the motion along X is described by

$$F_{\ell}(X) = \frac{1}{(\pi a_x^2)^{\frac{1}{4}}} \frac{1}{\sqrt{2^{\ell} \ell!}} H_{\ell}(\zeta) e^{-\zeta^2/2}, \quad (22d)$$

where H_{ℓ} is the Hermite polynomial, ℓ is the harmonic quantum number, $\ell = 0, 1, 2, \dots$

$$a_x = \sqrt{\frac{\hbar\omega_x}{K_x}}, \quad \omega_x = \sqrt{\frac{K_x}{M_{\text{Au}}}}. \quad (22e)$$

The corresponding energy levels depend on two quantum number, $n = 2\nu + |m|$ and ℓ ,

$$\varepsilon_{n\ell} = \hbar\omega_r \left(n + 1 \right) + \hbar\omega_x \left(\ell + \frac{1}{2} \right). \quad (23)$$

When ω_r and ω_x are incommensurate, the degeneracy of the level (n, ℓ) is $(n+1)(2s+1)$. For the values of K_x and K_r given by Eq. (20), $\hbar\omega_x = 1.24$ meV, $\hbar\omega_r = 4.87$ meV, $a_x = 0.13$ Å and $a_r = 0.07$ Å. Then the energy of the ground state is $\varepsilon_{00} = 5.49$ meV. The quantum state with $m = 5$ has the excitation energy $5\hbar\omega_r = 24.35$ meV which is of order of the ultraviolet cut off.

III. Direct Exchange Interaction between CNT QD electron and the Caged Atom

In order to calculate the exchange interaction between the gold atom and the itinerant electrons in the CNT we neglect the deviation of the gold atom from the equilibrium position $\mathbf{R} = (0, 0)$. Such a small deviation results in a small variation of the calculated exchange coupling as calculated below. The exchange interaction is determined mainly by the Coulomb repulsion between the CNT itinerant electron and the outer 6s electron of the gold atom. These two electrons can form singlet and triplet states and the corresponding energies are determined by Hund rules. When the implanted gold atom is placed on the CNT axis, the singlet-triplet energy splitting $V_{\text{exch}} = \varepsilon_T - \varepsilon_S$ due to the direct exchange interaction between the caged atom and the CNT wall is,

$$V_{\text{exch}} = -2 \int d^3\mathbf{r} d^3\mathbf{r}' \psi_{\text{CNT}}^*(\mathbf{r}) \psi_6^*(\mathbf{r}') \frac{e^2}{|\mathbf{r} - \mathbf{r}'|} \psi_{\text{CNT}}(\mathbf{r}') \psi_6(\mathbf{r}). \quad (24)$$

Here $\psi_6(\mathbf{r})$ is the wave function of the 6s-electron in the atom of gold and $\psi_{\text{CNT}}(\mathbf{r})$ is the wave function of electron in the CNT QD. In order to calculate the latter we need to recall the formalism for calculating electron wave function in CNT.

A zigzag CNT is specified by two basic vectors \mathbf{a}_1 and \mathbf{a}_2 , and a chiral vector \mathbf{c}_N ,

$$\mathbf{c}_N = N\mathbf{a}_1, \quad (25)$$

where N is integer and $|\mathbf{a}_1| = |\mathbf{a}_2| = a_0 = 2.46$ Å. A CNT is obtained by rolling a 2D graphene sheet such that the atom at the origin coincides with the atom at \mathbf{c}_N . Then $|\mathbf{c}_N| = 2\pi r_0$ is the length of the CNT circumference and r_0 is the CNT radius [see Figure 8].

The coordinates of atoms of the sub-lattice A or B are,

$$\begin{aligned}\mathbf{R}_{An_2} &= n_1\mathbf{a}_1 + n_2\mathbf{a}_2 + \frac{\mathbf{d}_1}{2} = (X_{An_2}, Y_{n_1 + \frac{n_2}{2}}), \\ \mathbf{R}_{Bn_2} &= n_1\mathbf{a}_1 + n_2\mathbf{a}_2 - \frac{\mathbf{d}_1}{2} = (X_{Bn_2}, Y_{n_1 + \frac{n_2}{2}}),\end{aligned}$$

where

$$X_{An_2} = \frac{a_0}{2\sqrt{3}} + \frac{3n_2a_0}{2\sqrt{3}}, \quad X_{Bn_2} = -\frac{a_0}{2\sqrt{3}} + \frac{3n_2a_0}{\sqrt{3}}, \quad Y_n = na_0. \quad (26)$$

Here x -axis is along the CNT axis and the y -axis is in the circumference direction. Then n_2 changes from 1 to N and we have the periodicity condition $Y_{n+N} = Y_n$. For the CNT to be semiconductor, N is not an integer multiplier of 3. We consider here the CNT with $N = 8$ and $r_0 = 3.13$ nm.

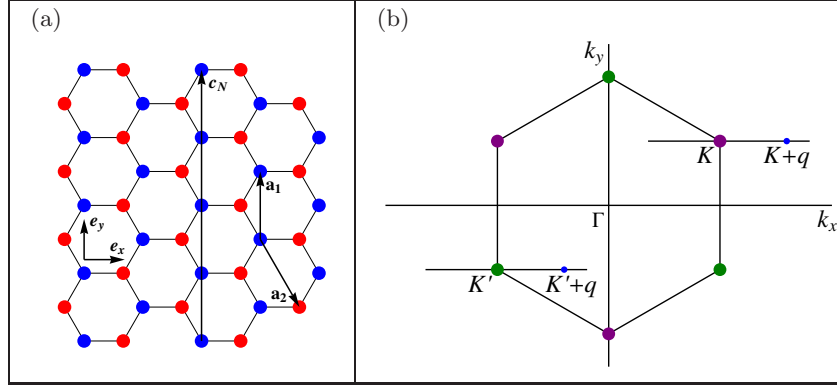


FIG. 8: (Color online) **Panel (a)**: A monoatomic layer of graphene. The red and blue dots denote carbon atoms of the sub-lattice A and B . The primitive vectors of graphene are \mathbf{a}_1 and \mathbf{a}_2 . The nanotube is obtained by choosing the chiral vector $\mathbf{c}_N = N\mathbf{a}_1$. The unit vectors \mathbf{e}_x and \mathbf{e}_y are fixed in the CNT in such a way that \mathbf{e}_x is along the CNT axis, and \mathbf{e}_y is along the circumferential direction \mathbf{c}_N . **Panel (b)**: The first Brillouin zone of graphene. k_x is the component of the 2D wave vector \mathbf{k} along the CNT axis and k_y is the component of \mathbf{k} in the circumferential direction. The green and purple dots denote the corners \mathbf{K} and \mathbf{K}' of the first BZ. The lines q denote the component of the wave vector \mathbf{k} along the CNT axis measured with respect to the corners \mathbf{K} and \mathbf{K}' .

The wave function of the lowest-energy quantum state of the CNT QD of the length $2h$ (i.e., for $|X_{A,Bn_2}| \leq h$) is

$$\begin{aligned}\psi_{\text{CNT}}(\mathbf{r}) &= \frac{1}{\sqrt{N}} \sum_{n_1 n_2} \Phi(\mathbf{r} - \mathbf{R}_{An_2}) \sin\left(\frac{\pi(h + X_{An_2})}{2h}\right) e^{i(K+q_N)Y_{n_1 + \frac{n_2}{2}}} + \\ &+ \frac{1}{\sqrt{N}} \sum_{n_1 n_2} \Phi(\mathbf{r} - \mathbf{R}_{Bn_2}) \sin\left(\frac{\pi(h + X_{Bn_2})}{2h}\right) e^{i(K+q_N)Y_{n_1 + \frac{n_2}{2}}},\end{aligned} \quad (27)$$

where $\Phi(\mathbf{r})$ is a Wannier function,

$$K = \frac{4\pi}{3a_0}, \quad q_N = \frac{2\pi\mu}{3Na_0}, \quad (28)$$

where $N = 3M + \mu$ with M being integer and $\mu = \pm 1$. μ is chosen in such a way that $(K + q_N)Na_0$ be integer multiplier of 2π .

The Wannier functions $\Phi(\mathbf{r} - \mathbf{R})$ and $\Phi(\mathbf{r} - \mathbf{R}')$ with $\mathbf{R} \neq \mathbf{R}'$ are orthogonal one to another, so that the wave function (27) is normalized by the condition,

$$\int d^3\mathbf{r} |\psi_{\text{CNT}}(\mathbf{r})|^2 = 1.$$

The wave function $\psi_{\text{CNT}}(\mathbf{r})$ vanishes when $|x| > h$. The term q_N is introduced to satisfy the Bohr-Sommerfeld quantization rule which says that $(K + q_N)Na_0$ is an integer multiplier of 2π .

In what following, we consider the following model wave function,

$$\psi_{\text{CNT}}(\mathbf{r}) = \frac{\mathcal{N}_{\text{CNT}}}{\sqrt{\pi h}} \sin\left(\frac{\pi(h+x)}{2h}\right) e^{i(Kr_0+\nu)\phi} e^{-\frac{|r-r_0|}{a_C}}, \quad (29)$$

where $\mathbf{r} = (x, r, \phi)$ are cylindrical coordinates, $\nu = \frac{h}{3}$ [see Eq. (28)], $a_C = 0.80 \text{ \AA}$ is the radius of the carbon atom. The normalization factor \mathcal{N}_{CNT} is

$$\mathcal{N}_{\text{CNT}} = \frac{2}{\sqrt{a_C(4r_0 + a_C e^{-\frac{2r_0}{a_C}})}} \approx \frac{1}{\sqrt{a_C r_0}}.$$

As for $\psi_6(\mathbf{r})$, the wave function of the 6s-electron in the gold atom, we will use the following model wave function,

$$\psi_6(\mathbf{r}) = \frac{1}{\sqrt{\pi a_{\text{Au}}^3}} e^{-\frac{\sqrt{x^2+r^2}}{a_{\text{Au}}}}, \quad (30)$$

where $a_{\text{Au}} = 1.35 \text{ \AA}$ is the atomic radius of gold.

Substituting the wave function (29) into eq. (24), we get

$$V_{\text{exch}} = -\frac{2}{\pi h a_{\text{Au}}^3 a_C r_0} \int_{-h}^h dx dx' \int_0^\infty r dr r' dr' \mathcal{G}(x, x', r, r') \mathcal{F}(x, x', r, r'), \quad (31)$$

where

$$\mathcal{G}(x, x', r, r') = \sin\left(\frac{\pi(h+x)}{2h}\right) \sin\left(\frac{\pi(h+x')}{2h}\right) e^{-\frac{|r-r_0|+|r'-r_0|}{a_C}} e^{-\frac{1}{a_{\text{Au}}}(\sqrt{x^2+r^2}+\sqrt{x'^2+r'^2})}, \quad (32)$$

$$\mathcal{F}(x, x', r, r') = \int_0^{2\pi} d\phi d\phi' \frac{e^{-i(Kr_0+\nu)(\phi-\phi')}}{\sqrt{(x-x')^2 + r^2 + r'^2 - 2rr' \cos(\phi-\phi')}}. \quad (33)$$

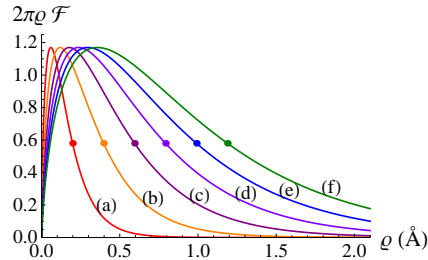


FIG. 9: (Color online) The function $2\pi\rho\mathcal{F}(x + \frac{1}{2}\rho \cos \varphi, x - \frac{1}{2}\rho \cos \varphi, r + \frac{1}{2}\rho \sin \varphi, r - \frac{1}{2}\rho \sin \varphi)$ as functions of ρ for different values of r . Curves (a) – (f) correspond to $r = 0.5, 1, 1.5, 2, 2.5, 3 \text{ \AA}$. The dots denote the half-maximum of the function.

The function $\mathcal{F}(x, x', r, r')$ depends on $x - x'$ but not on $x + x'$. It has its maximum at $x - x' = 0$ and $r - r' = 0$, decreases with $\rho = \sqrt{(x - x')^2 + (r - r')^2}$ and vanishes when $\rho \gg \rho_c$ exceeds some critical value ρ_c . Numerical calculations plotted in Fig. 9 show that $\rho_c \lesssim 1.2 \text{ \AA}$. The function $\mathcal{G}(x, x', r, r')$ varies slowly with $x - x'$ and $r - r'$. Therefore, we can approximate $\mathcal{F}(x, x', r, r')$ by the following expression,

$$\mathcal{F}(x, x', r, r') = \mathcal{F}_0(r) \delta(r - r') \delta(x - x'), \quad (34)$$

where

$$\mathcal{F}_0(r) = \int_{-\infty}^{\infty} dx' \int_{-\infty}^{\infty} dr' \mathcal{F}\left(x + \frac{x'}{2}, x - \frac{x'}{2}, r + \frac{r'}{2}, r - \frac{r'}{2}\right). \quad (35)$$

Integration of the RHS of Eq. (35) yields,

$$\mathcal{F}_0(r) = \frac{32\pi^2 r}{99}.$$

Then the exchange interaction (31) can be written as,

$$V_{\text{exch}} = -\frac{64\pi}{99ha_{\text{Au}}^3 a_C r_0} \int_{-h}^h dx \sin^2\left(\frac{\pi(h+x)}{2h}\right) \int_0^\infty r^3 dr e^{-\frac{2|r-r_0|}{a_C}} e^{-\frac{2}{a_{\text{Au}}}\sqrt{x^2+r^2}}. \quad (36)$$

For $a_C = 0.8 \text{ \AA}$, $a_{\text{Au}} = 1.35 \text{ \AA}$, $r_0 = 3.13 \text{ \AA}$ and $h = 5r_0 = 15.65 \text{ \AA}$, $V_{\text{exch}} \approx -43.3 \text{ meV}$. The exchange interaction is ferromagnetic which agrees with the Hund rules.

IV. Absence of electron tunneling between the CNT and the Caged Atom

The tunneling rate T between the atom and the CNT can be estimated as,

$$V_t = \int d^3\mathbf{R} |\Psi_{000}^{\text{Au}}(\mathbf{R})|^2 \int d^3\mathbf{r} \Psi_{\text{CNT}}^*(\mathbf{r}) \frac{e^2}{|\mathbf{r} + \mathbf{R}|} \psi_6(\mathbf{r}), \quad (37)$$

where the electronic wave functions $\Psi_{\text{CNT}}(\mathbf{r})$ and $\psi_6(\mathbf{r})$ are given by Eqs. (29) and (30), and the atomic wave function $\Psi_{000}^{\text{Au}}(\mathbf{R})$ is defined by Eq. (22). Using cylindrical coordinates $\mathbf{r} = (x, r, \phi)$ and $\mathbf{R} = (X, R, \varphi)$, we get

$$V_t = \frac{1}{\sqrt{\pi a_{\text{Au}}^3 h a_C r_0}} \int_{-h}^h dx \sin\left(\frac{\pi(h+x)}{2h}\right) \int_{-\infty}^{\infty} dX F_0^2(X) \int_0^\infty r dr e^{-\frac{1}{a_C}|r-r_0|} e^{-\frac{1}{a_{\text{Au}}}\sqrt{x^2+r^2}} \int_0^\infty R dR \Phi_{00}^2(R) \\ \times \int_0^{2\pi} d\varphi \frac{e^2}{\sqrt{(x-X)^2 + r^2 + R^2 + 2rR \cos \varphi}} \int_0^{2\pi} d\phi e^{i(Kr_0 + \nu)\phi}.$$

Taking into account that $Kr_0 + \nu$ is non-zero integer, we get $V_t = 0$.

V. Derivation of the Scaling Equations

In this subsection we describe the derivation of the scaling equations as displayed in the main text around Eqs. (8-12) therein. In order to carry out the poor man's scaling analysis, let us divide the energy interval $|\epsilon| < D$ ("conduction band") into three intervals (see Fig. 10):

- i. $-D + \delta D < \epsilon - \epsilon_F < D - \delta D$,
- ii. $D - \delta D < \epsilon - \epsilon_F < D$,
- iii. $-D < \epsilon - \epsilon_F < -D + \delta D$.

The quantum states within the interval (i) are retained and the quantum states within the intervals (ii) and (iii) are to be integrated out.

The corrections to H_K due to the virtual scattering are shown in Figs. 11 and 12. Here the solid blue lines describe the quantum state of the quantum dot. The dashed purple lines with a red circle at one side describe falling or scattered conduction electron and dashed purple lines with two red circles at the ends describe virtual conduction electron within the energy interval (i). The dashed and dotted violet lines with arrow right or left correspond to virtual electron with energy within the interval (ii) or (iii).

The contribution of the second order diagram in Fig. 11(a) is,

$$\delta K_{\epsilon_q \epsilon_{q'}}^{(2a)} = -\frac{\delta D}{D} \left(K_{\epsilon_q D} K_{D \epsilon_{q'}} + \frac{3}{16} J_{\epsilon_q D} J_{D \epsilon_{q'}} \right) \rho(D), \quad (38a)$$

$$\delta J_{\epsilon_q \epsilon_{q'}}^{(2a)} = -\frac{\delta D}{D} \left(K_{\epsilon_q D} J_{D \epsilon_{q'}} + J_{\epsilon_q D} K_{D \epsilon_{q'}} + \frac{1}{2} J_{\epsilon_q D} J_{D \epsilon_{q'}} \right) \rho(D). \quad (38b)$$

The contribution of the second order diagram in Fig. 11(b) is,

$$\delta K_{\epsilon_q \epsilon_{q'}}^{(2b)} = \frac{\delta D}{D} \left(K_{\epsilon_q -D} K_{-D \epsilon_{q'}} + \frac{3}{16} J_{\epsilon_q -D} J_{-D \epsilon_{q'}} \right) \rho(-D), \quad (38c)$$

$$\delta J_{\epsilon_q \epsilon_{q'}}^{(2b)} = \frac{\delta D}{D} \left(K_{\epsilon_q -D} J_{-D \epsilon_{q'}} + J_{\epsilon_q -D} K_{-D \epsilon_{q'}} - \frac{1}{2} J_{\epsilon_q -D} J_{-D \epsilon_{q'}} \right) \rho(-D). \quad (38d)$$

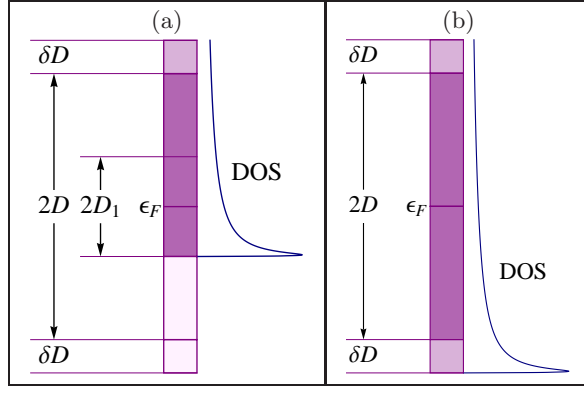


FIG. 10: (Color online) The particle and hole states which are integrated out from the conduction band on reducing the bandwidth by δD for $D > D_1$ [panel (a)] and $D < D_1$ [panel (b)]. The curve denotes the density of states (DOS).

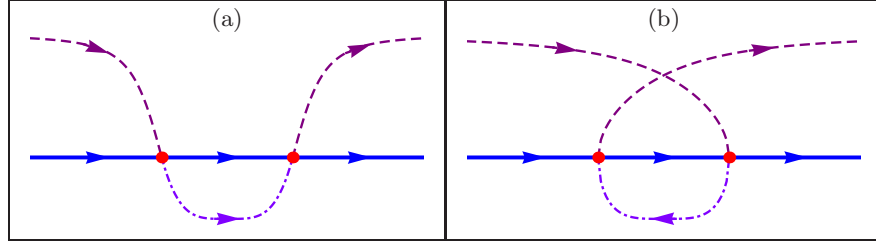


FIG. 11: (Color online) Second order electronic [panel (a)] and hole [panel (b)] diagrams which have a particle in an intermediate state at a band edge (dashed and dotted line).

It should be taken into account that $\rho(-D) = 0$ when $D > D_1$, so that the diagram in Fig. 11(b) contributes to H_K just when $D < D_1$.

The contribution of the third order diagram in Fig. 12(a) is,

$$\delta K_{\epsilon_q \epsilon_{q'}}^{(3a)} = -\frac{\delta D}{D} K_{\epsilon_q \epsilon_{q'}} \left(8k^2 + \frac{3}{2} j^2 \right) \frac{1}{D} \int_{-D}^0 d\epsilon \vartheta(-\epsilon) \vartheta(\epsilon + D_1),$$

$$\delta J_{\epsilon_q \epsilon_{q'}}^{(3a)} = \frac{\delta D}{D} J_{\epsilon_q \epsilon_{q'}} \left(-4k^2 + j^2 \right) \frac{1}{D} \int_{-D}^0 d\epsilon \vartheta(-\epsilon) \vartheta(\epsilon + D_1).$$

After integration over ϵ , we get,

$$\delta K_{\epsilon_q \epsilon_{q'}}^{(3a)} = -\frac{\delta D}{D} K_{\epsilon_q \epsilon_{q'}} \left(8k^2 + \frac{3}{2} j^2 \right) \frac{\min(D, D_1)}{D}, \quad (39a)$$

$$\delta J_{\epsilon_q \epsilon_{q'}}^{(3a)} = \frac{\delta D}{D} K_{\epsilon_q \epsilon_{q'}} \left(-4k^2 + j^2 \right) \frac{\min(D, D_1)}{D}. \quad (39b)$$

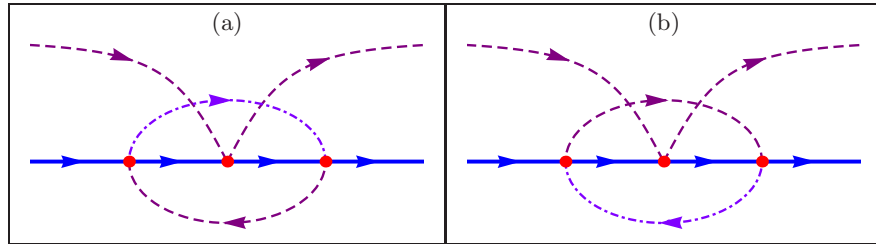


FIG. 12: (Color online) Third order electronic [panel (a)] and hole [panel (b)] diagram with a particle in an intermediate state at a band edge (dashed and dotted line) which results in the over-screened fixed point.

Similarly, the contribution of the third order diagram in Fig. 12(b) is,

$$\delta K_{\epsilon_q \epsilon_{q'}}^{(3b)} = \frac{\delta D}{D} K_{\epsilon_q \epsilon_{q'}} \left(8k^2 + \frac{3}{2} j^2 \right) \vartheta(D_1 - D), \quad (39c)$$

$$\delta J_{\epsilon_q \epsilon_{q'}}^{(3b)} = \frac{\delta D}{D} K_{\epsilon_q \epsilon_{q'}} \left(4k^2 + j^2 \right) \vartheta(D_1 - D). \quad (39d)$$

Combining Eqs. (38) and (39), we get the scaling equations for the dimensionless couplings k and j . For $D \gg D_1$, the equations are

$$\delta k = -\frac{\delta D}{D} \left(k^2 + \frac{3j^2}{16} \right), \quad (40a)$$

$$\delta j = -\frac{\delta D}{D} \left(2kj + \frac{j^2}{2} \right). \quad (40b)$$

Approximating

$$D \frac{\delta k}{\delta D} \approx \frac{\partial k}{\partial \ln D}, \quad D \frac{\delta j}{\delta D} \approx \frac{\partial j}{\partial \ln D},$$

we get Eqs. (8a) and (8b) of the main text. Similarly, for $D < D_1$ we get $\delta k = 0$ and

$$\delta j = -\frac{\delta D}{D} \left(j^2 - 2j^3 \right). \quad (41)$$

The last equation yields Eq. (10) of the main text.